tvst

https://doi.org/10.1167/tvst.8.4.6

Article

Automatic Characterization of Retinal Blood Flow Using OCT Angiograms

Omer Aharony[1,*], Orly Gal-Or[2,3,*], Asaf Polat[2,3], Yoav Nahum[2,3], Dov Weinberger[2,3], and Yair Zimmer[1]

[1] School of Medical Engineering, Afeka College of Engineering, Tel Aviv, Israel
[2] Department of Ophthalmology, Rabin Medical Center, Petah Tikva, Israel
[3] Sackler Faculty of Medicine, Tel Aviv University, Tel Aviv, Israel

Correspondence: Yair Zimmer, School of Medical Engineering, Afeka College of Engineering, 38 Mivtza Kadesh Street, Tel Aviv 6998812, Israel. e-mail: yairz@afeka.ac.il

Received: 25 September 2018
Accepted: 21 May 2019
Published: 15 July 2019

Keywords: optical coherence tomography angiography; vascular quantification; vessel density; fractal dimension; foveal avascular zone

Citation: Aharony O, Gal-Or O, Polat A, Nahum Y, Weinberger D, Zimmer Y. Automatic characterization of retinal blood flow using OCT angiograms. Trans Vis Sci Tech. 2019;8(4):6, https://doi.org/10.1167/tvst.8.4.6

Purpose: To quantitatively characterize the retinal vascular network in healthy and pathological cases using optical coherence tomography angiography (OCTA) images.

Methods: The study included 56 eyes of 28 patients as follows: 26 healthy, 20 with diabetic retinopathy (DR), 6 with age-related macular degeneration (AMD), and 4 with retinal vein occlusion (RVO). For 33 eyes (16 healthy and 17 with DR), vessel density maps were provided by the OCTA machine. An automatic algorithm classified the image (as healthy, DR, AMD, or RVO) and provided quantitative information obtained from the angiograms, including global vessel density, global fractal dimension, and fovea avascular zone (FAZ) area. Classification results were compared with the diagnosis made by a retina specialist. The quantitative values were compared with the literature and to values provided by the OCTA machine.

Results: The success rate of classification was 83.9%. Vessel densities obtained by our algorithm (in healthy and DR cases) were significantly lower than the values reported in previous studies using OCTA. Similarly, they were much lower than the values provided by the OCTA machine. However, vessel densities in the healthy cases were similar to or higher than (depending on the retinal layer) the recently published values that may be considered as gold standard. Our values of fractal dimension were similar to those previously reported.

Conclusions: Our algorithm provides significantly improved vessel density values compared with previous studies. We believe our algorithm successfully omits false vessels.

Translational Relevance: Accurately assessing retinal vessel density enables better evaluation of retinal disorders.

Introduction

Optical coherence tomography angiography (OCTA) is a noninvasive technique that can detect blood flow signal in retinal and choroidal vessels using motion contrast. It compares the decorrelation signal (differences in the backscattered OCT signal intensity) between sequential OCT B-scans taken at the same cross-section; thus, yielding maps of vascular flow. OCTA provides size and localization information, visualizing the retinal and the choroidal vasculature.[1]

Numerous studies described how to automatically detect and classify retinal disorders (e.g., diabetic retinopathy [DR]). However, most of them relied on fundus images[2–5] rather than on OCT images or OCT angiograms. Recent development in OCTA induced attempts to use advanced image processing in order to extract quantitative information that characterizes the vascular network in the retina from the angiograms. In particular, parameters, such as vessel density and fractal dimension, were computed in several studies.[6–11] Fractal dimension can be seen as a measure of the roughness or abruptness of changes in a curve or a surface. A network of blood vessels in an image generates gray level changes in the image, and thus can be characterized by the fractal dimension.

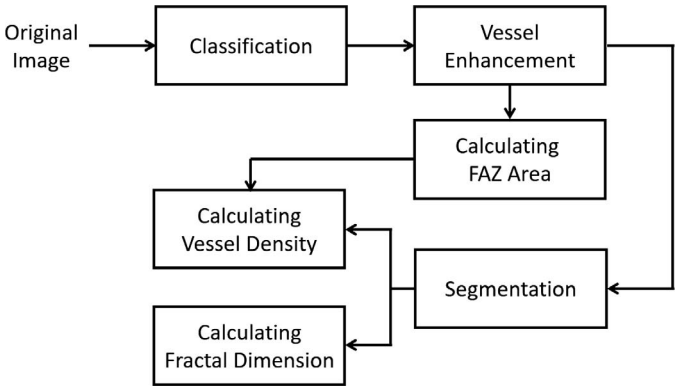

Figure 1. A Schematic description of the algorithm.

Currently, several commercial OCTA machines can provide, in addition to the angiogram, rough values of the global and local vessel density. Anegondi et al.[12] compared the vascular features obtained using the following three different machines: AngioVue (Optovue, Inc., Fremont, CA), SSOCT Angio (Topcon Systems, Tokyo, Japan), and AngioPlex (Carl Zeiss Meditec, Jena, Germany). The results showed that in the superficial retinal layer vessel density was similar among all three devices, but in the deep retinal layer the vessel density obtained from the AngioVue machine was significantly higher than the one obtained using the other two machines.

In this study, we proposed an automatic algorithm that analyses OCT angiograms of the retina. The algorithm first classified the input image checking the following four possible conditions: healthy, DR, age-related macular degeneration (AMD), and retinal vein occlusion (RVO). Classification was performed based on the gray level statistical parameters of the image. Then, the image was automatically enhanced and segmented. Next, came calculating the area of the foveal avascular zone (FAZ), the vessel density, and the Hausdorff fractal dimension. Both the vessel density and the fractal dimension were calculated globally on the entire image, and the results were used to characterize the global retinal blood flow and vasculature.

Classification results were compared with the diagnosis made by a retina specialist. The obtained values for the vessel density were compared with the literature and to the automatic results provided by the OCTA machine used (AngioVue). The values obtained for the fractal dimension were compared with the literature.

The main contribution of the proposed method is obtaining an improved description of retinal vasculature and consequently an improved assessment of the vessel density due to significantly reducing the amount of false blood vessels in the resulted image.

Methods

As described above, the proposed method was composed of classification followed by several image processing steps and then calculation of quantitative parameters characterizing retinal vasculature.

The entire algorithm, whose various steps are detailed below, is schematically described in Figure 1.

Image Acquisition

A retrospective observational study was conducted in 28 patients. Data on background, clinical, and additional tests were collected from the medical records. The study followed the tenets of the 2013 declaration of Helsinki and was approved by the Institutional Ethics Review Board of Rabin Medical Center.

All the images analyzed in our study were obtained using the AngioVue OCTA machine (Optovue, Inc., Fremont, CA). Each image contained 600×600 pixels representing an area of 3×3 mm centered on the fovea.

The collected data included images of 56 eyes as follows: 26 healthy eyes, 20 eyes with DR, 6 eyes with AMD, and 4 eyes with RVO.

Each OCTA scan enabled the analysis of retinal and choroidal vasculature: superficial capillary plexus, deep capillary plexus, outer retina, and choriocapillaris. For 33 cases (16 healthy eyes and 17 eyes with DR), vessel density maps provided by the machine were also available.

Classification

In order to associate the image with the relevant disorder (healthy, DR, AMD, or RVO), statistical parameters (mean, standard deviation, skewness, and kurtosis) of its gray level histogram were calculated for each automatically obtained layer of the patient's retina. In statistics, skewness is a measure of the asymmetry of the distribution. Kurtosis is a measure of the shape of the distribution and shows whether it is uniform or has a sharp peak. The expressions for the four statistical parameters are provided below:

$$\mu = \sum_i i \cdot p(i) \quad , \quad \sigma^2 = \sum_i (i-\mu)^2 \cdot p(i)$$

$$s = \frac{1}{\sigma^3} \sum_i (i-\mu)^3 \cdot p(i) \quad ,$$

$$k = \left(\frac{1}{\sigma^4} \sum_i (i-\mu)^4 \cdot p(i) \right) - 3 \qquad (1)$$

where: μ, σ^2, s, and k are the mean, variance, skewness, and kurtosis, respectively; and $p(i)$ is the probability of a pixel to contain a gray level i.

Using these parameters, a range of values defining each pathology was first set.

The values for a specific pathology were essentially the minimal and maximal values that were found for each layer and parameter among the images related to this pathology in our data set.

When an image of a retinal layer is analyzed, the algorithm compares the obtained values of the four statistical parameters with the range of values predefined for each disorder. The layer is associated with a category only if the values of all four parameters fit the predefined range of this class (a layer may be linked to more than a single class due to the partial overlap between the ranges of values related to different categories). This process is repeated for all four layers. The case would be diagnosed as belonging to a specific category (healthy, DR, AMD, or RVO) only if it was related to this category in all four layers (i.e., the whole set of 4 statistical parameter in all the layers fit the range corresponding to this category). When a case is diagnosed as belonging to two different classes, both diagnoses are presented. When a case does not fit any category, it is considered as "no diagnosis." We did not have such a case in our data set.

Vessel Enhancement

In order to calculate the vessel density and the Hausdorff fractal dimension, the image must first be filtered in order to achieve vessel enhancement. To do so, the Frangi vesselness filter[13] was applied on the input image. This filter performs a type of contrast enhancement, which emphasizes structures (such as blood vessels) that can be regarded as tubular.

It should be mentioned that the filter introduced by Frangi fits a case in which the tubular objects are darker than their surroundings. In OCT angiograms the blood vessels appear as bright tubular objects, and therefore the filter was applied on the negative of the images.

Segmentation

Following vessel enhancement, the obtained image was thresholded in order to get a binary image presenting retinal vasculature in white and the rest of the image in black. The threshold value was determined using Otsu's method,[14] which selects the optimal threshold by maximizing the between-class variance.

The resulted image is used for calculating vessel density as well as the Hausdorff fractal dimension.

Calculating FAZ Area

In case the image was classified as healthy, the following algorithm was applied. First, the image obtained after applying the vesselness filter was convolved with a Gaussian for smoothing. For the superficial capillary plexus layer $\sigma = 8.5$ was used, and for the deep capillary plexus layer $\sigma = 5.5$ was used. These values were determined by trial and error. Next, the result was converted to a binary image, taking the mean gray level of the smoothed image as the threshold. Due to the strong smoothing, which blurred the gaps between blood vessels, the only bright region in the thresholded image belonged to the FAZ. Then, binary morphological dilation with a 5-pixel-long diamond-shaped structuring element (SE) was applied to expand the FAZ shape to the correct size (this SE can be described in the following way using a 5×5 square: top and bottom rows: "00100," 2nd and 4th rows: "01110," middle row: "11111"). The result is a binary image in which the FAZ is the area covered by bright pixels.

Calculating FAZ size using an automatic algorithm was unreliable in cases of severe pathology, where the FAZ merges with flow-less areas in the retina, as a result of hemorrhage or ischemia. In order to overcome this difficulty, an average FAZ size was calculated for each of the pathologies using a semiautomatic algorithm on the entire pathological data.

Each image was first filtered using the vessel enhancement method that was described above. Next, smoothing by a Gaussian filter followed by thresholding and binary dilation were performed on the vessel-enhanced image. The standard deviation of the Gaussian, the value of the threshold for segmentation and the structuring element for dilation were chosen manually for each image in order to obtain optimal results. The above process was repeated for the entire pathological data set: 20 cases of DR, six cases of AMD, and four cases of RVO, for both superficial

and deep layers. Finally, for each of the pathologies an average FAZ size was determined as the mean of the data obtained by the above process.

Calculating Vessel Density

Vessel density is calculated on the binary image resulted from the steps described above in the "Segmentation" subsection. The vessel density is provided by the following expression:

$$Density = \frac{B}{T - F} \quad (2)$$

where B is the number of bright pixels in the binary image, T is the total number of pixels in the binary image, and F is the number of pixels representing the FAZ. In cases diagnosed as healthy, F is computed from the input image as described above in the first paragraph of the "Calculating FAZ Area" subsection. In cases diagnosed as pathological, F is constant and changes according to the pathology (refer to the last paragraph of the "Calculating FAZ Area" subsection above).

Calculating the Fractal Dimension

Similar to the vessel density, the fractal dimension is computed on the binary image obtained after the segmentation step described above. The Hausdorff fractal dimension is calculated using the box counting method[15,16] on the entire image.

The box counting method divides the image into boxes of size r, and counts the number of boxes $N(r)$ that contain even a small part of the structure. Next the box size r is divided to half and box counting is performed again. This will repeat until the box size is one pixel. Then, a linear fit between $\log(N(r))$ and $\log(1/r)$ is performed. The Hausdorff fractal dimension is determined as the slope of the line (in absolute value).

Results

Classification

Based on the gray level statistical parameters, our method successfully classified 47 of 56 cases. All AMD cases were correctly diagnosed. Of 20 cases of DR, one was diagnosed as both DR and healthy. Of four cases of RVO, three cases had two diagnoses: one case was diagnosed as both RVO and healthy, and two cases were diagnosed as both RVO and DR. From 26 healthy cases, five were diagnosed as both healthy and DR.

It was expected always to obtain the correct diagnosis because our criteria for classification were based on the value taken from the entire database. However, demanding intersection (i.e., logical "AND" condition) between several criteria in order to classify a case reduced significantly the ambiguity in the diagnosis (cases associated to two groups). As stated above, 47 of 56 cases were uniquely diagnosed, which means a success rate of 83.9%. Only two pathological cases were also classified as healthy (false negative), and five healthy cases were also classified as pathological (false positive). This gives a sensitivity of 93.7% and a specificity of 83.8%.

It should be pointed out that the accuracy of the classification method is limited for AMD and RVO due to the small number of cases used for constructing the classification criteria.

Calculating FAZ Area

The algorithm for finding the FAZ in both healthy and pathological cases was described above in the Methods section. Figure 2 shows examples of the obtained results in the superficial capillary plexus layer for a heathy case (Fig. 2a) and for two cases of DR (Figs. 2b, 2c). Figure 2b refers to a case of nonproliferative diabetic retinopathy (NPDR), while Fig. 2c shows a case of proliferative diabetic retinopathy (PDR). For all three cases, the boundary of the FAZ is displayed in red. It should be mentioned that the FAZ obtained for the superficial capillary plexus layer using the automatic algorithm is often more accurate than the FAZ obtained for the deep retinal capillary plexus layer.

The values obtained in this study (all 56 eyes) for the area of the FAZ are presented in Table 1.

Calculating Vessel Density

Vessel density was calculated for the entire set of 56 cases. Table 2 provides the obtained results.

The P values for the various pathologies, which were calculated using an unpaired t-test, refer to the separation from healthy cases.

We observed, as expected, that the mean values obtained for healthy cases are higher than the corresponding ones in the pathological cases. Furthermore, the vessel density in the superficial capillary plexus layer is lower than in the deep capillary plexus layer. The P values in Table 2 show that the

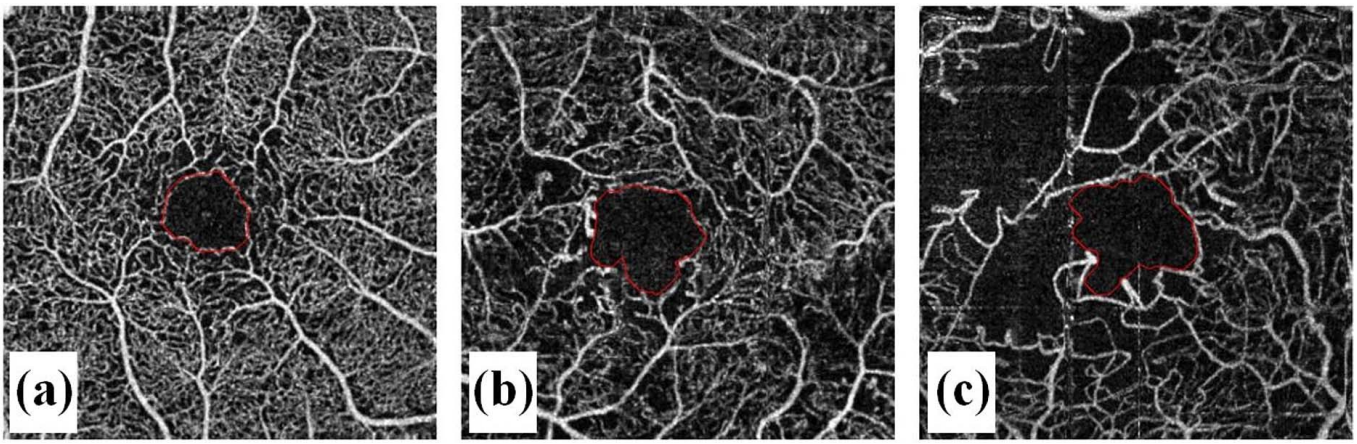

Figure 2. The FAZ boundary (*red*) on top of the OCT angiogram. (a) Healthy, (b) NPDR, and (c) PDR.

separation between healthy cases and pathological cases is statistically significant for all the pathologies.

Calculating Fractal Dimension

The Hausdorff fractal dimension was calculated for the entire set of 56 cases. Table 3 provides the obtained results. The *P* values for the various pathologies, which were calculated using an unpaired *t*-test, refer to the separation from healthy cases.

It can be seen that the mean values obtained for healthy cases are, as expected, higher than the ones obtained for pathological cases. The *P* values in Table 3 show that the separation between healthy cases and pathological cases is statistically significant for all the pathologies. Because the healthy cases seem to form a narrower distribution than the distribution of DR cases, we also used the Wilcoxon rank sum test and confirmed that healthy cases are separated from DR cases.

Comparison with Previous Studies and Machine Results

The values of the vessel density obtained for healthy eyes were compared with the values described in previous studies[7,8,17,18] that used OCTA, as detailed in Table 4. A similar comparison was performed for DR cases, as presented in Table 5. Tables 4 and 5 show that the values obtained from our algorithm are significantly lower than the ones reported in the literature.

Our results for the vessel density were also compared with the study by Rabiolo et al.,[11] which compared several image processing methods for quantifying the retinal vessel density. Rabiolo et al.[11] obtained a wide range of mean vessel density values depending on the segmentation method used, both for the superficial capillary plexus layer (35.1%–51.6% for healthy subjects and 33.9%–43.5% for DR patients) as well as for the deep capillary plexus layer (31.7%–46.4% for healthy subjects and 20.8%–42.2% for DR patients). When comparing to their results using Otsu thresholding (the most similar method to ours), we can conclude from Table 6 that our values of vessel density are only slightly lower than the values obtained by Rabiolo et al.[11]

The AngioVue machine can automatically compute global and local values of the vessel density. We compared the values obtained by our algorithm with the vessel density of the superficial capillary plexus computed by the machine for 16 healthy and 17 DR cases. The obtained results are presented in Table 7.

It can be seen that for both the healthy as well as the DR cases, the vessel density obtained by our algorithm is significantly lower than the one provided by the OCTA machine. The difference between the two density values (machine provided, algorithm obtained) was calculated for each case and the results

Table 1. The Area of the FAZ (in mm^2)

	Healthy	DR	AMD	RVO
Superficial capillary plexus layer	0.25 ± 0.08	0.22 ± 0.08	0.22 ± 0.06	0.25 ± 0.03
Deep capillary plexus layer	0.44 ± 0.09	0.41 ± 0.11	0.42 ± 0.20	0.35 ± 0.13

Table 2. Vessel Density (%)

	Healthy	DR	AMD	RVO
Superficial capillary plexus layer	34.90 ± 3.64	26.18 ± 6.68 $P < 0.0001$	28.09 ± 1.96 $P < 0.0001$	31.32 ± 4.63 $P < 0.05$
Deep capillary plexus layer	39.53 ± 3.42	27.54 ± 7.15 $P < 0.0001$	31.11 ± 2.88 $P < 0.0001$	29.51 ± 5.71 $P < 0.0001$

Table 3. Fractal Dimension

	Healthy	DR	AMD	RVO
Superficial capillary plexus layer	1.71 ± 0.02	1.66 ± 0.05 $P < 0.0001$	1.68 ± 0.01 $P < 0.0001$	1.69 ± 0.03 $P < 0.02$
Deep capillary plexus layer	1.73 ± 0.01	1.66 ± 0.05 $P < 0.0001$	1.69 ± 0.02 $P < 0.0001$	1.68 ± 0.03 $P < 0.0001$

Table 4. Vessel Density in Healthy Eyes (%): Comparison with Previous Studies

	Our Method	Bhanushali et al.[7]	Kim et al.[8]	Dimitrova et al.[17]	Zahid et al.[18]
Superficial capillary plexus layer	34.90 ± 3.64	49.7 ± 0.55	42.60 ± 1.90	41.53 ± 14.08	55.56 ± 1.69
Deep capillary plexus layer	39.53 ± 3.42	53.1 ± 0.73	43.30 ± 0.90	51.39 ± 13.05	60.58 ± 1.50

Table 5. Vessel Density in DR (%): Comparison with Previous Studies

	Our Method	Bhanushali et al.[7]	Kim et al.[8]
Superficial capillary plexus layer	26.18 ± 6.68	39.2 ± 1.21 (mild NPDR)	38.2 ± 3.9 (mild NPDR)
		40.1 ± 0.58 (moderate NPDR)	—
		38.5 ± 0.76 (severe NPDR)	34.9 ± 5.6 (severe NPDR)
		38.9 ± 1.38 (PDR)	33.3 ± 4.0 (PDR)
Deep capillary plexus layer	27.54 ± 7.15	39.7 ± 1.57 (mild NPDR)	42.5 ± 1.5 (mild NPDR)
		40.2 ± 0.53 (moderate NPDR)	—
		39.4 ± 0.68 (severe NPDR)	40.6 ± 5.1 (severe NPDR)
		39.2 ± 0.94 (PDR)	39.9 ± 3.9 (PDR)

Table 6. Vessel Density (%): Comparison with Rabiolo et al.[11]

Capillary Plexus Layer	Our Method	Rabiolo et al.[11]
Healthy		
Superficial	34.90 ± 3.64	38.8 ± 2.2
Deep	39.53 ± 3.42	40.7 ± 2.0
DR		
Superficial	26.18 ± 6.68	35.8 ± 3.5
Deep	27.54 ± 7.15	30.3 ± 4.3

were averaged. The obtained range of differences was 18.63±2.84% for healthy eyes and 17.94±4.80% for DR cases.

Our results for healthy eyes can also be compared with the values described in the recently published study of Yu et al.[19] who used confocal imaging to assess the macular microvasculature density in human donor eyes. According to their study, the vessel density in the superficial capillary plexus layer is 31% on average (between 29% and 33% in various regions of the macula) and in the deep capillary plexus layer it is 17% on average (between 14% and 20% in various

Table 7. Vessel Density (%): Comparison with Machine Results

	Our Method	AngioVue Machine
Healthy	35.25 ± 3.19	53.88 ± 1.86
DR	27.59 ± 6.63	45.53 ± 5.21

macular regions). In our study (Tables 2 and 4), vessel density in healthy cases was 34.90±3.64% for the superficial capillary plexus layer and 39.53±3.42% for the deep capillary plexus layer. We can see that for the superficial capillary plexus layer our results are similar to those obtained by Yu et al.,[19] while for the deep capillary plexus layer our results are significantly higher than the ones presented by Yu et al.[19] in their study.

The values of the fractal dimension obtained for healthy and for DR cases were compared with the values described in two previous studies, as detailed in Table 8.

One can see that the mean values obtained for the fractal dimension by our algorithm are similar to the ones provided in the previous studies. For healthy cases, our mean values are almost identical to the values provided by Kim et al.[8]

Discussion

We have seen that the values obtained by our algorithm for the vessel density are significantly lower than the ones obtained from OCT angiograms in previous studies (Tables 4, 5). One exception was the study by Rabiolo et al.,[11] which yielded similar results to ours using a similar segmentation method (Otsu thresholding). It should be noted that, using a method entitled "multilevel," Rabiolo et al.[11] obtained for the deep capillary plexus layer values of vessel density which were even lower than ours. Although this method was quite different from ours, it involved image processing with a Hessian filter, which may have a similar effect on the images as the vesselness filter we used for contrast enhancement.

In addition, our results for the vessel density were much lower than the ones provided by the AngioVue machine. Obtaining significantly lower results compared both with the results of the machine as well as to previous studies seems to indicate that our algorithm provides underestimated values. However, it is known that OCT angiograms contain noise, which can generate false flow signal that can be interpreted as small blood vessels.[20] We believe that our algorithm (that combines vessel enhancement using the vesselness filter and Otsu thresholding) successfully handles false flow signals. This is supported by the comparison with the results of Yu et al.[19] (who used confocal microscopy rather than OCTA), which showed that for healthy subjects our algorithm yielded vessel densities that are either similar to (in the superficial capillary plexus layer) or higher than (in the deep capillary plexus layer) those Yu et al.[19] obtained.

As an illustrative demonstration, Figures 3 and 4 present for three cases both the original OCT angiogram and the binary image (after segmentation and filtering) from which the vessel density was computed in our algorithm. Figure 3 shows the superficial capillary network layer, while Figure 4 shows the deep capillary plexus layer for the same cases. In each figure, the original OCT angiograms are shown in the top row and the binary images are displayed in the bottom row. Both figures refer to the

Table 8. Fractal Dimension in Healthy and in DR: Comparison with Previous Studies

	Our Method	Kim et al.[8]	Zahid et al.[18]
Superficial capillary plexus layer			
Healthy	1.713 ± 0.017	1.717 ± 0.006	1.638 ± 0.045
DR	1.656 ± 0.046	1.695 ± 0.018 (mild NPDR) 1.673 ± 0.038 (severe NPDR) 1.665 ± 0.026 (PDR)	1.563 ± 0.077
Deep capillary plexus layer			
Healthy	1.731 ± 0.013	1.730 ± 0.004	1.719 ± 0.040
DR	1.662 ± 0.045	1.726 ± 0.007 (mild NPDR) 1.713 ± 0.035 (severe NPDR) 1.712 ± 0.020 (PDR)	1.599 ± 0.113

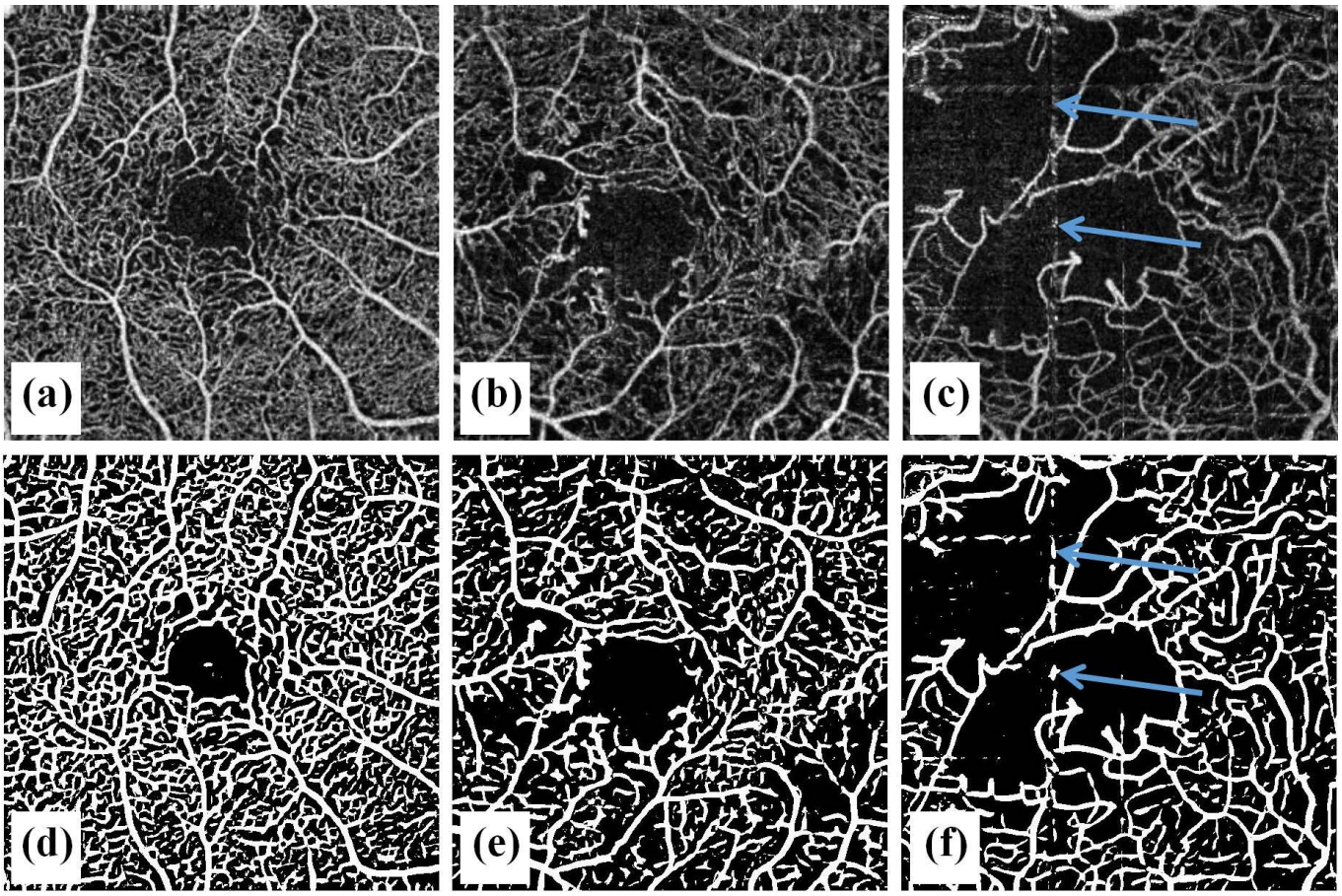

Figure 3. (a–c) En face angiogram of the superficial capillary plexus layer network of healthy (a), NPDR (b), and PDR (c) eyes. (d–f) Corresponding binary image generated by our algorithm of healthy (d), NPDR (e), and PDR (f) eyes. The *broken vertical line* indicated by *blue arrows* in (c) and in (f) is an artifact.

three cases already shown in Figure 2 (left column – healthy, middle column – NPDR, right column – PDR).

Using our algorithm, a significant amount of noise was removed from the image, hence reducing the numeric value of the obtained vessel density. It seems that in the healthy case and in the PDR case the retinal vasculature is well described by the binary image, while in the NPDR case some of the small blood vessels are lost (leading to an underestimated vessel density).

If we focus on the superficial capillary plexus layer (for which vessel densities provided by the scanner were available), even in the NPDR case the vessel density obtained from our algorithm (31%) seems to be to fairly accurate compared with the value provided by the machine (41.25%). To see that, one should compare the original NPDR image (Fig. 3b) with the binary image of the healthy case (Fig. 3d), which represents an algorithm-provided vessel density of 42%. The density mismatch between these two images shows that a vessel density of 42% (close to the value of 41.25% provided by the machine for the NPDR case) is significantly overestimated. Turning to the PDR case, a vessel density of 25% (provided by the algorithm) seems closer to reality than 37% (the value given by the machine).

One should note that when applying our vessel density algorithm to compute vessel density in pathological cases using an average value of the FAZ area (based on all the cases) an error occurs in the obtained value. Based on the typical size of the FAZ, we estimate this error is in the range of 1% to 2%.

Finally, it must be emphasized that our study included only eyes with DR, RVO, and AMD. Thus, our OCTA algorithm findings are confined to those

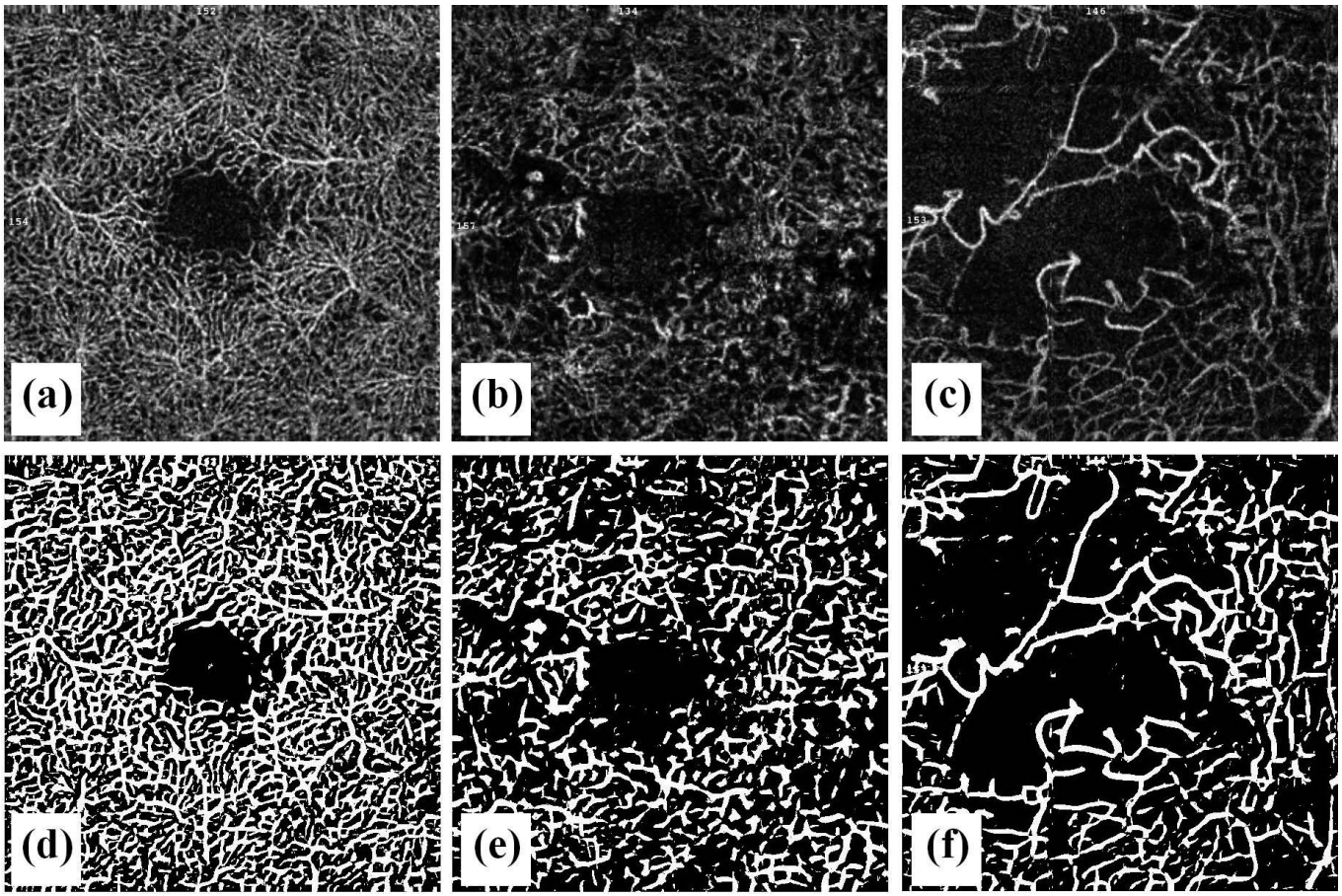

Figure 4. (a–c) En face angiogram of the deep capillary plexus layer network of healthy (a), NPDR (b), and PDR (c) eyes. (d–f) Corresponding binary image generated by our algorithm of healthy (d), NPDR (e), and PDR (f) eyes. The figure refers to the same cases shown in Figure 3.

pathologies only. Future work should be encouraged to study the OCTA finding in other pathologies.

Conclusions

In this study, an automatic algorithm that calculates quantitative parameters that characterize the retinal blood flow from OCT angiograms was developed. Both vessel density and Hausdorff fractal dimension for the entire image were calculated in healthy and in pathological cases. The vessel density values we calculated by the algorithm were significantly lower than the values that appear in the literature as well as those provided by the OCTA machine. We believe this reflects, at some extent, a reduced influence of false signal of blood vessels on the result. The success rate of classification by the algorithm is 83.9%, and it can be improved by collecting more data.

Acknowledgments

Disclosure: **O. Aharony**, None; **O. Gal-Or**, None; **A. Polat**, None; **Y. Nahum**, None; **D. Weinberger**, None; **Y. Zimmer**, None

*OA and OG-O contributed equally to this article.

References

1. de Carlo TE, Romano A, Waheed NK, Duker JS. A review of optical coherence tomography angiography (OCTA). *Int J Retina Vitreous*. 2015;1:1–15.
2. Abramoff MD, Niemeijer M, Russell SR. Automated detection of diabetic retinopathy: barriers to translation into clinical practice. *Expert Rev Med Devices*. 2010;7:287–296.

3. Faust O, Acharya UR, Ng EY, Ng KH, Suri JS. Algorithms for the automated detection of diabetic retinopathy using digital fundus images: a review. *J Med Syst*. 2012;36:145–157.
4. Valverde C, Garcia M, Hornero R, Lopez-Galvez MI. Automated detection of diabetic retinopathy in retinal images. *Indian J Ophthalmol*. 2016;64: 26–32.
5. Soomro TA, Gao J, Khan T, Hani AFM, Khan MAU, Paul M. Computerized approaches for the detection of diabetic retinopathy using retinal fundus images: a survey. *Pattern Anal Appl*. 2017; 20:927–961.
6. Gadde GKS, Anegondi NS, Bhanushali DR, et al. Quantification of vessel density in retinal optical coherence tomography angiography images using local fractal dimension. *Invest Ophthalmol Vis Sci*. 2016;57:246–252.
7. Bhanushali D, Anegondi N, Gadde SGK, et al. Linking retinal microvasculature features with severity of diabetic retinopathy using optical coherence tomography angiography. *Invest Ophthalmol Vis Sci*. 2016;57:OCT519–OCT525.
8. Kim AY, Chu Z, Shahidzadeh A, Wang RK, Puliafito CA, Kashani AH. Quantifying microvascular density and morphology in diabetic retinopathy using spectral-domain optical coherence tomography angiography. *Invest Ophthalmol Vis Sci*. 2016;57:OCT362–OCT370.
9. Chu Z, Lin J, Gao C, et al. Quantitative assessment of the retinal microvasculature using optical coherence tomography angiography, *J Biomed Opt*. 2016;21(6):066008.
10. Al Sheikh M, Falavarjani KG, Akil H, Sadda SR. Impact of image quality on OCT angiography based quantitative measurements. *Int J Retina Vitreous*. 2017;3:1–6.
11. Rabiolo A, Gelormini F, Sacconi R, et al. Comparison of methods to quantify macular and peripapillary vessel density in optical coherence tomography angiography. *PLoS One* 2018; 13:e0205773.
12. Anegondi N, Kshirsagar A, Mochi TB, Roy AS. Quantification comparison of retinal vascular features in optical coherence tomography angiography images from three different devices. *Ophthalmic Surg Lasers Imaging Retina*. 2018; 49:488–496.
13. Frangi AF, Niessen WJ, Vincken KL, Virgever ML. Multiscale vessel enhancement filtering. *Medical Image Computing and Computer-Assisted Intervention—MICCAI'98*. Lecture notes in Computer Science. Berlin: Springer-Verlag; 1998:130–137.
14. Otsu N. A threshold selection method from gray-level histograms. *IEEE Trans Syst Man Cybernet*. 1979;9:62–66.
15. Arakawa K, Krotov EP. Estimating fractal dimension from range images of natural terrain. New York: Carnegie Mellon University; 1991.
16. Łabędź P, Ozimek A, Ozimek P. Box-counting dimension in landscape photographs analysis. In: Buhmann E, Kieferle J, Pietsch M, Paar P, Kretzler E, eds. *Digital Landscape Architecture 2009*: *Proceedings at Anhalt University of Applied Sciences*. Bernburg: Anhalt University of Applied Sciences; 2009:142–149.
17. Dimitrova G, Chihara E, Takahashi H, Amano H, Okazaki K. Quantitative retinal optical coherence tomography angiography in patients with diabetes without diabetic retinopathy. *Invest Ophthalmol Vis Sci*. 2017;58:190–196.
18. Zahid S, Dolz-Marco R, Freund KB, et al. Fractal dimensional analysis of optical coherence tomography angiography in eyes with diabetic retinopathy. *Invest Ophthalmol Vis Sci*. 2016;57: 4940–4947.
19. Yu PK, Mammo Z, Balaratnasingam C, Yu DY. Quantitative study of the macular microvasculature in human donor eyes. *Invest Ophthalmol Vis Sci*. 2018;59:108–116.
20. Spaide RF, Fujimoto JG, Waheed NK, Sadda SR, Staurenghi G. Optical coherence tomography angiography. *Prog Retin Eye Res*. 2018;64:1–55.